

Structural properties of faint low surface brightness galaxies

Isha Pahwa,^{1*} and Kanak Saha^{1†}

¹*Inter-University Centre for Astronomy and Astrophysics, Ganeshkhind, Post Bag 4, Pune 411007, India*

draft

ABSTRACT

We study the structural properties of Low Surface Brightness galaxies (LSB) using a sample of 263 galaxies observed by the Green Bank Telescope (Schneider et al. 1992). We perform 2D decompositions of these galaxies in the SDSS g , r and i bands using the GALFIT software. Our decomposition reveals that about 60% of these galaxies are bulgeless i.e., their light distributions are well modelled by pure exponential disks. The rest of the galaxies were fitted with two components: a Sersic bulge and an exponential disk. Most of these galaxies have bulge-to-total (B/T) ratio less than 0.1. However, of these 104 galaxies, 20% have $B/T > 0.1$ i.e., hosting significant bulge component and they are more prominent amongst the fainter LSBs. According to $g-r$ colour criteria, most of the LSB galaxies in our sample are blue, with only 7 classified as red LSBs. About 15% of the LSB galaxies (including both blue and red) in our sample host stellar bars. The incidence of bars is more prominent in relatively massive blue LSB galaxies with very high gas fraction. These findings may provide important clues to the formation and evolution of LSB galaxies - in particular on the bar/bulge formation in faint LSB disks.

Key words: galaxies: photometry — galaxies: evolution — galaxies: structure — galaxies:spiral

1 INTRODUCTION

The last two decades have witnessed a significant increase in the population of low surface brightness (hereafter, LSB) galaxies due to wide-field surveys such as the Sloan Digital Sky Survey (York et al. 2000, SDSS), as well as due to advancement in new techniques in observational astronomy allowing one to dig deeper in the sky (Kniazev et al. 2004; Zhong et al. 2008; Rosenbaum et al. 2009; Galaz et al. 2011; Blanton et al. 2011; Duc et al. 2015; Trujillo & Fliri 2016; Greco et al. 2017). This growing number of LSB population suggests that they might hold a significant fraction of baryon repositories in the local universe (Impey & Bothun 1997; McGaugh et al. 1995b) although they occupy the faint end of the galaxy luminosity function (Impey et al. 1988; Bothun et al. 1985). In fact, the number density of LSB galaxies is comparable to that of the high surface brightness (hereafter, HSB) galaxies (McGaugh et al. 1995b; O’Neil & Bothun 2000; O’Neil et al. 2003a). But the formation and evolution of these LSB galaxies remained unclear and are

thought to have taken a different route than the HSB galaxies.

There are several indications such as low star-formation rates (van der Hulst et al. 1993; Schombert et al. 2011), low metallicities (McGaugh & Bothun 1994; de Blok & van der Hulst 1998; Kuzio de Naray et al. 2004), sparse H- α emission (Pickering et al. 1997; Huang et al. 2014) suggesting that LSB galaxies are under-evolved system compared to their HSB counterparts (Bothun et al. 1997). In general, these LSB galaxies are known to have high neutral hydrogen gas to stellar mass ratios, associated with nearly non-detection or little CO molecules (O’Neil et al. 2003b; Honey et al. 2018) - indicating their inefficiency in converting the gas to stars. Although the exact reason remains to be understood, the combination of low surface density and dark matter dominance at all radii, as derived from the observed rotation curve (de Blok & McGaugh 1996; de Blok et al. 2001) makes sure that the disk instabilities are unlikely to set in. In fact, using analytical and numerical simulations which include gas and cold dark matter components, it has been shown that the realistic models of LSB galaxies are stable against local and global instabilities (Mihos et al. 1997; Mayer & Wadsley 2004; Ghosh & Jog 2014). In other words, LSB galaxies would be unlikely to host strong bars and spiral

* E-mail: ipahwa@iucaa.in

† E-mail: kanak@iucaa.in

features as reflected in earlier observations by [McGaugh & Bothun \(1994\)](#); [Impey et al. \(1996\)](#) who found bar fraction to be only a few percent. But several recent studies seem to indicate a growing bar fraction from $\sim 8\%$ ([Honey et al. 2016](#)) to about 20% in [Cervantes Sodi & Sánchez García \(2017\)](#) as larger samples of LSB galaxies are being analyzed. If such a trend continues, one needs to rethink about the evolution of normal LSB galaxies.

Previous studies that have explored in detail the properties of LSB galaxies are mostly late-type disk dominated ([de Blok et al. 1995](#); [McGaugh & Bothun 1994](#)) or Malin-type giant LSBs ([Sprayberry et al. 1995](#); [Pickering et al. 1997](#)). Over the last ten years, this notion seems to be changing as HST revealed an insightful picture of Malin1 - the very inner part has a bar and a bulge ([Barth 2007](#)) - like in a normal HSB galaxy. A similar conclusion was derived by [Lelli et al. \(2010\)](#) who found Malin1 to have a normal HSB like inner disk. A number of other LSBs are reported to host bulges whose stellar populations, colours and gas kinematics are remarkably similar to those hosted by HSB galaxies ([Beijersbergen et al. 1999](#); [Galaz et al. 2006](#); [Pizzella et al. 2008](#); [Morelli et al. 2012](#)) - indicating the LSBs might be having a parallel formation sequence to the HSB galaxies. This has prompted us to investigate the two component bulge-disk decomposition of a sample of LSB galaxies that remained relatively unexplored in the literature.

In the present work, we choose a sample of LSB galaxies observed by the Green Bank Telescope (GBT) as given in [Schneider et al. \(1992\)](#) to study the structural properties of LSB galaxies. We perform two component bulge-disk decomposition of 294 LSB galaxies using GALFIT ([Peng et al. 2002, 2010](#)). Further based on visual inspection, the sample is divided into two groups - barred and unbarred and their properties are discussed in detail.

This paper is organised as follows. In Section 2, we present our galaxy sample. We also discuss the 2D decomposition steps and the method to obtain the structural parameters in this section. The results are presented in Section 3. Lastly, we discuss and summarize the conclusions in Section 5.

2 SAMPLE SELECTION AND METHOD

2.1 The GBT/SDSS Sample

The Uppsala General Catalog of galaxies ([Nilson 1973](#), UGC) consists of a list of dwarf and LSB galaxies which was assembled by Nilson in 1973. This catalog covers all northern galaxies ($\delta \geq -2^{\circ}30'$) visible on the Palomar Sky Survey with a blue diameter larger than $1'$. In the nineties, a group led by S. E. Schneider used this sample to map the neutral hydrogen of dwarf and other low surface brightness (LSB) galaxies such as irregular, Sd-m etc. This selection of galaxies by S. E. Schneider brings an incompleteness of $\sim 14\%$ in the sample. His group took neutral hydrogen observations in two steps. First, they used Arecibo telescope for the galaxies in the declination range $-2^{\circ} \leq \delta \leq 38^{\circ}$. They reported 762 dwarf or LSB galaxies with this telescope ([Schneider et al. 1990](#)). In the second step, they used Green Bank telescope (GBT) for galaxies in the declination range, $\delta \geq 38^{\circ}$ along with a number of galaxies farther

south for flux comparisons with Arecibo observations and to search for extended halos, totalling 633 galaxies ([Schneider et al. 1992](#)). We choose their sample of 633 galaxies to analyse the detailed structural properties. The sample completeness is discussed in [Schneider et al. \(1990, 1992\)](#); [Thuan et al. \(1991\)](#); [Dominguez-Tenreiro et al. \(1996\)](#) who have also studied the spatial clustering and their relationship to bright galaxies.

The GBT sample of 633 galaxies is retrieved from NASA/IPAC EXTRAGALACTIC DATABASE (NED) which provides the *ra*, *dec*, redshift *z* etc. ([Schneider et al. 1992](#)). We cross-match this sample with SDSS ([York et al. 2000](#)) data release 13 ([SDSS Collaboration et al. 2016](#), DR13) and find 354 galaxies for which spectroscopic redshifts are available. Finally, we have visually inspected images in *r* and *g* bands of each of these galaxies to remove from the sample those galaxies which are drastically affected by a merger or a companion and also those galaxies where the presence of a bright star is affecting the analysis. These are a total of 19 in number. We have also removed 35 edge-on galaxies from sample. In addition to them, we have also rejected 6 galaxies having star-forming clumps in them. This has further reduced our sample to 294 galaxies that are common between GBT and SDSS. These galaxies are in the redshift range of 0.001-0.037.

In order to compare our LSB sample with other disk galaxies on the colour magnitude plane, we use the [Simard et al. \(2011\)](#) catalog which is based on SDSS DR7. In particular, we use their bulge-disk decomposition parameters where bulges are fitted with free Sersic indices. We extract galaxies in the same redshift range as of our sample. This final sample consists of 70810 galaxies for which we have *r*-band absolute magnitudes, redshifts and bulge-to-disk ratios. We call this sample as “all galaxy sample”.

2.2 Multi-band Bulge-Disk Decomposition

The images of 294 galaxies are drawn from the SDSS *g* (green), *r* (red) and *i* (near-infrared) filters with effective central wavelengths being 4770, 6231 and 7625 Å. The SDSS Science Archive Server provides the survey images for these galaxies, called “corrected frames” which are identified by a unique name and it’s a combination of run number, the camera column and the frame sequence number. Figure 1 shows the *r*-band images of some of these galaxies with mix morphologies e.g., spirals, irregulars from our sample. These images are calibrated in nanomaggies per pixel, and have a sky-subtraction applied. From each frame, a 2-4 arcmin cutout from the central coordinate of the galaxy is extracted depending upon the galaxy’s redshift. It ensures that an average galaxy size covers at least 50% of the total area.

Before we proceed to discuss the bulge-disk decomposition, we decontaminate these 294 (in each of the three bands) galaxies to remove the surrounding sources around the target galaxy in the cutout. For removing these unwanted sources, each galaxy image cutout is considered separately and the pixel values of each unwanted source are replaced with the average value of the pixels surrounding that source. This is done using the Image Reduction and Analysis Facility (IRAF) IMEDIT task, which creates a circular annulus of a chosen radius around the central coordinates of

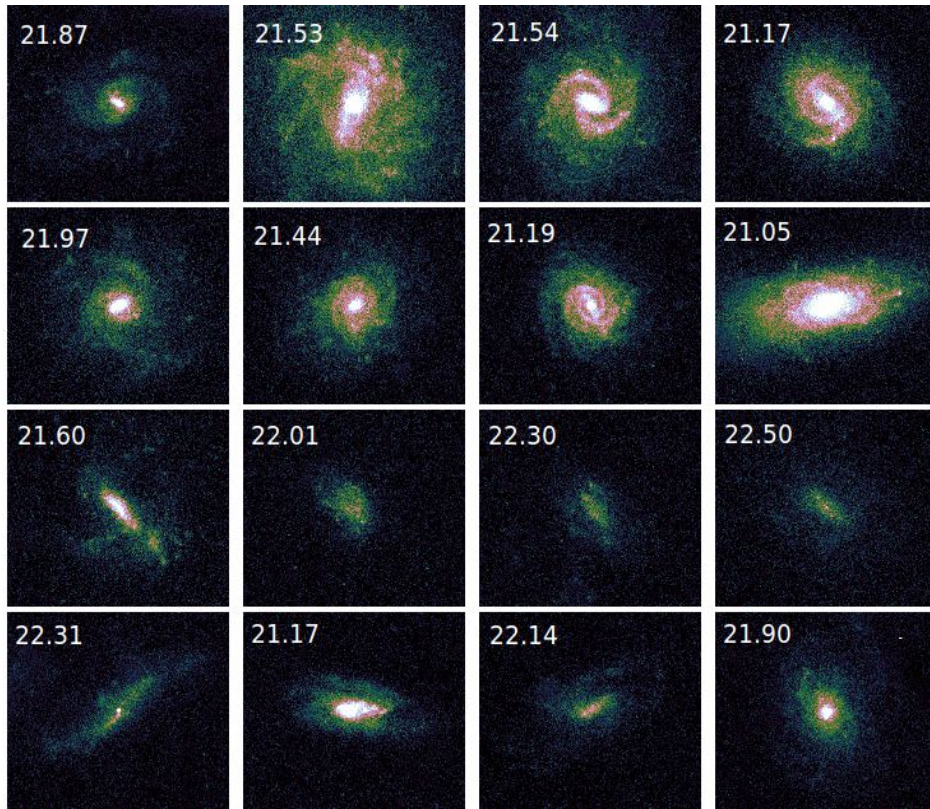


Figure 1. A few representative galaxies of different morphologies in our sample in r -band. The disk central surface brightness (in units of $\text{mag}/\text{arcsec}^2$) is indicated on the top of each galaxy. The colour scale is same for all images.

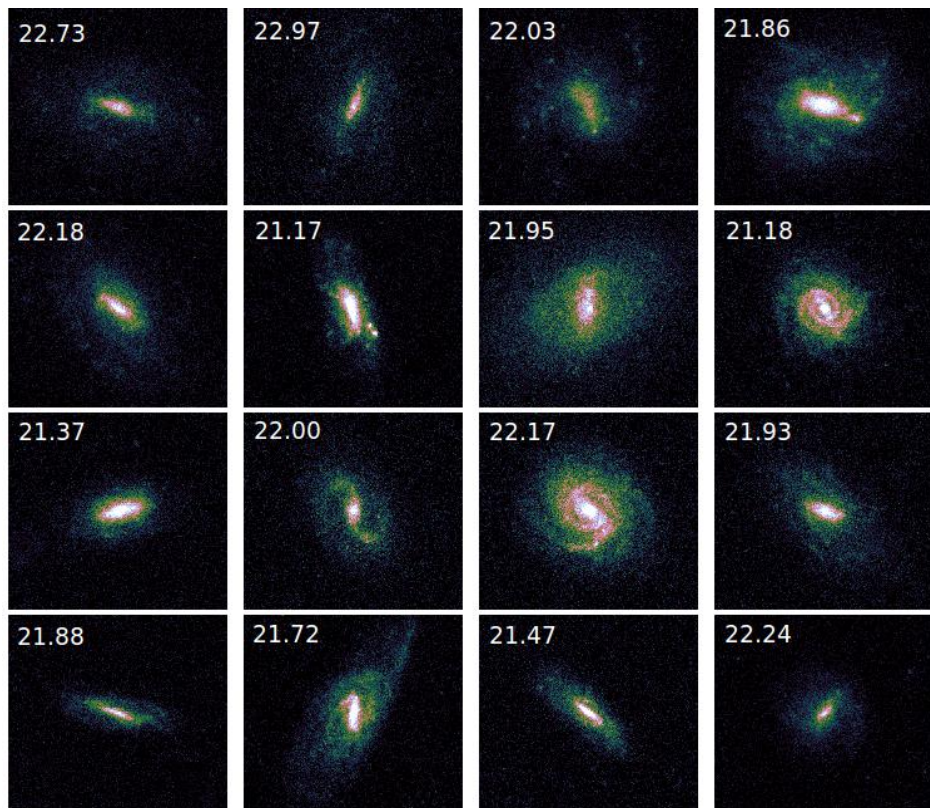


Figure 2. Same as in Figure 1 but here we have chosen to show only barred galaxies in our sample.

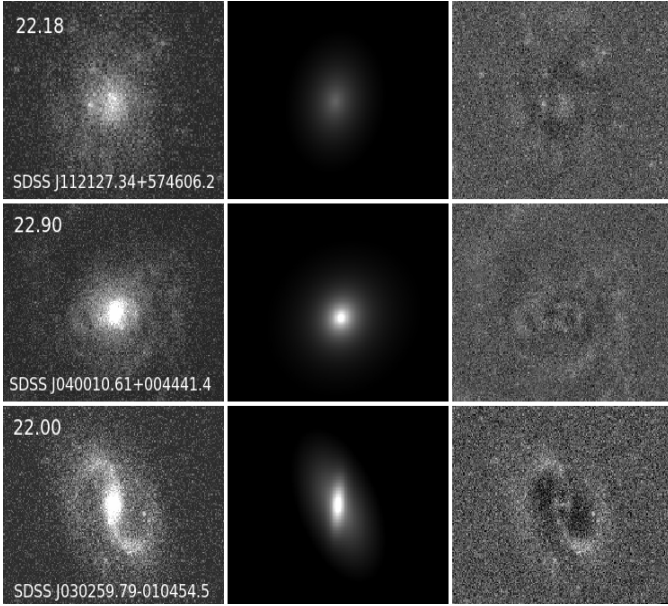


Figure 3. Three examples of bulge-disk decompositions using GALFIT. The first column shows the r -band observation images of the selected galaxies, the second column shows the GALFIT model images and the third column shows the residual images which are basically the subtraction of model images from the observation images. The three selected galaxies are *typical* examples of irregular, bulge and bar galaxies. The disk central surface brightness and SDSS IDs are indicated on the top of each galaxy.

the selected source and replaces the pixels in this circle with the background values.

Once the cutouts are cleaned, we perform two-dimensional bulge-disk decomposition on each galaxy image using the GALFIT (version 3.0.5) software (Peng et al. 2002, 2010). This software models the light distribution using the analytic functions, known as parametric fitting which adjusts the parameters in the analytic functions to try and match with the shape and profile of galaxies. For more details about the fitting algorithm and the usage of GALFIT, the reader is advised to go through Peng et al. (2002, 2010).

We start with by fitting two components, i.e., bulge and disk profiles to the light distribution of each galaxy in r -band. We adopt the standard Sersic and the exponential profiles for the bulge and disk components of the galaxy, respectively (Sersic 1968; Freeman 1970). These are discussed as follows -

- The Sersic profile has the following functional form:

$$I(R) = I_e \exp \left\{ -b_n \left[\left(\frac{R}{R_e} \right)^{1/n} - 1 \right] \right\}, \quad (1)$$

where $I(R)$ is the pixel surface brightness at a radius R from the centre of a galaxy, the parameter R_e is known as the effective radius such that half of the total flux is within R_e and I_e is the pixel effective surface brightness at the effective radius R_e and the parameter n is the Sersic index that controls the shape of the light profile. The dependent-variable b_n is coupled to n and is given as $b_n = 1.9992n - 0.3271$ (Graham & Driver 2005), thus it is not a free parameter.

- The exponential profile for the disk is given by:

$$I(R) = I_0 \exp \left(-\frac{R}{R_s} \right), \quad (2)$$

where I_0 is the central surface brightness, R_s is the scale length of the stellar disk.

The full profile is the addition of the Sersic and the exponential profiles. Bars in the sample are included in the bulge light and are not dealt separately. To run the GALFIT successfully, we need to provide the point spread function (PSF). To generate PSF images for SDSS observations, a Gaussian profile with a given Full Width at Half Maximum (FWHM) of the surface brightness distribution is fit with GALFIT. The FWHMs for SDSS observations are obtained from Science Archive Server. The background image (also known as σ image) is generated internally.

In addition, the GALFIT software also requires initial guesses of parameters of bulge and disk profiles which we choose from SDSS such as ra , dec , $PetroMag_r$, $PetroMag_g$, $PetroMag_i$, $deVAB_r$, $expAB_r$, $deVPhi_r$, $expPhi_r$. After setting the initial parameters, we run the GALFIT for all 294 galaxies in r -band. The output of the GALFIT fitting returns the final model of the galaxy and the residual image which is formed by the subtraction of the final model from the original image. All the residuals are visually inspected to see whether the final model obtained is a good fit to the original image or not. On the basis of residual inspection and bad reduced χ^2 values, we do not include 31 galaxies in our study. As mentioned earlier in this section, we have rejected few galaxies having star-forming clumps around the centre. This was also done based on the visual inspection. As GALFIT was not able to fit them properly (reduced χ^2 was not good), the residuals of these type of galaxies had left-over bright sub-components which showed that these galaxies were having star-forming clumps. We thus do not include them in our study. Our final sample consists of 263 galaxies.¹ All the subsequent analysis and results presented in this paper are based on this specific sample. Based on the visual inspection in r and g bands, we have found 43 bars out of 294 galaxies i.e., $\sim 15\%$ are barred LSBs in our sample. In Figure 2, we show images of some representative barred LSBs in our sample. A discussion on the barred LSBs is presented in section 4.

The output of the GALFIT consists of three images -

- (i) The postage stamp sized region of the input image.
- (ii) The final model of the galaxy in that region.
- (iii) The residual image which is formed by subtracting the final model from the first image.

In Figure 3, we show the three examples of bulge-disk decompositions which we have obtained using GALFIT software. The three selected galaxies are *typical* examples of irregular, bulge and bar galaxies as shown in first, second and third row. The first column shows the r -band observation images of these selected galaxies, the second column shows

¹ The online supplementary material consists of GALFIT output for these 263 galaxies in our sample. For all these galaxies, reduced χ^2 is around one. The image and GALFIT fits are available on request.

the GALFIT model images and the third column shows the residuals images.

After fitting all the galaxies in our sample in r -band, we follow the same procedure to fit the galaxies in g and i bands. We make the cutouts accordingly and decontaminate them as described previously. We generate PSF using the same procedure. Now, we take the advantage of fitting the galaxies in r -band. We apply the results of r -band decompositions to the g and i bands decompositions by fixing all the parameters except for the positions of centres and the bulge and disk magnitudes of the galaxies. This technique, i.e., using results of one band into others as initial conditions, is known as “simultaneous fitting” technique and has been used extensively in literature (Simard et al. 2011; Lackner & Gunn 2012; Meert et al. 2015; Kim et al. 2016).

2.3 Structural parameters

The two-component decomposition by GALFIT provides us the basic photometric parameters of the bulge and disk components for each galaxy in our sample. These parameters are further used to derive quantities such as central surface brightness, colour of the galaxy etc. as explained below. We convert the model magnitude to AB magnitude system using standard relation (Oke 1974). All the magnitudes are then corrected for Galactic Extinction. Hereafter, all the magnitudes mentioned in this paper correspond to the AB magnitude system unless otherwise specifically mentioned.

The logarithmic central surface brightness for the disk component ($\mu_{0,\text{disk}}$) can be calculated as

$$\mu_{0,\text{disk}} = m_{\text{disk}} + 2.5 \log_{10}(2\pi R_s^2), \quad (3)$$

where m_{disk} refers to the apparent magnitude of the disk component of the galaxy. The total central surface brightness of the galaxy is given by

$$I_{\text{total}} = I_0 + I_e e^{b_n} \quad (4)$$

and the logarithmic total central surface brightness can be written as

$$\mu_{0,\text{total}} = \text{zpt} - 2.5 \log_{10} I_{\text{total}}. \quad (5)$$

The central surface brightness is then corrected for the inclination and the cosmological dimming effects by using the following equation (Zhong et al. 2008)

$$\mu_{0,\text{corrected}} = \mu_0 + 2.5 \log_{10}(b/a) - 10 \log_{10}(1+z). \quad (6)$$

Following on, we will always use “corrected” central surface brightness everywhere and thus we will drop the subscript “corrected” from the definition of μ_0 .

After estimating μ_0 in r and g bands, we calculate the approximate B -band central surface brightness by using the following transformation equation (Smith et al. 2002; Cervantes Sodi & Sánchez García 2017):

$$\mu_0(B) = \mu_0(g) + 0.47(\mu_0(g) - \mu_0(r)) + 0.17. \quad (7)$$

This will be used to classify our sample galaxies as LSBs as per the criterion given in B -band. One needs to be bit cautious here as it is an approximate transformation equation. It can aid to the uncertainty in the results.

The absolute magnitude, M is corrected against dust

extinction using K -correction as follows:

$$M = m - 5 \log_{10} \left(\frac{D}{10\text{pc}} \right) - K, \quad (8)$$

where m is the apparent magnitude of the galaxy, D is the distance to the galaxy in pc and K is the K -correction term that accounts for the difference to transfer from observed band to the rest-frame band. The correction term depends on the spectral energy distribution and hence on the redshift of the object (Hogg et al. 2002). The K -correction assumes a simple relation for a power-law continuum

$$K = -2.5(1 + \alpha_\nu) \log_{10}(1+z), \quad (9)$$

where α_ν is the slope of the continuum and has a canonical value of -0.5 (Schmidt & Green 1983; Boyle et al. 1988).

Figure 4 depicts the distribution of the absolute magnitudes of our sample galaxies in r , g and i bands, where the absolute magnitude refers to the total model magnitude obtained from our GALFIT analysis. Our sample galaxies cover a wide range of magnitudes, while some are as bright as $M_r \sim -21$; the dominant population of the galaxies are on the fainter side ($M_r \geq -19$) going upto about -14. The medians of distributions of the absolute magnitudes of our sample galaxies in r , g and i bands lie at -18.07, -17.71 and -18.26. It seems from this figure that these galaxies are overall more luminous in the i -band (i.e., near-infrared) by about 0.19-0.55 mag than in r and g bands (optical bands) which indicates the ageing of the existing stars in these galaxies.

3 DISTRIBUTION OF CENTRAL SURFACE BRIGHTNESS

The classification of a galaxy into a HSB or LSB is based on its disk central surface brightness ($\mu_{0,\text{disk}}$). A disk galaxy is called HSB if its B -band disk central surface brightness peaks at 21.56 mag/arcsec² (Freeman 1970). Disk galaxies whose disk central surface brightness is about 1 mag fainter, are termed as LSBs. According to this, we define LSB galaxies with $\mu_{0,\text{disk}} \geq 22.5$ mag/arcsec² in the B -band (McGaugh 1996; Rosenbaum et al. 2009).

A similar criterion has been adopted to classify a disk galaxy as an LSB in the r -band, i.e., $\mu_{0,\text{disk}}(r) = 21$ mag/arcsec² (Courteau 1996; Brown et al. 2001; Adami et al. 2006) and is $\sim 1.1\sigma$ away from the mean value of HSB galaxies as reported by Courteau (1996).

In the rest of this paper, we follow this r -band criterion to select LSB from our sample, i.e., a galaxy is termed as LSB whose $\mu_{0,\text{disk}} \geq 21$ mag/arcsec² in the r -band. Schneider et al. (1992) have already filtered out the LSB galaxies from the UGC catalog, however, we re-confirm this by plotting their distribution of disk central surface brightness in Figures 5 and 6.

3.1 Bulgeless LSB galaxies

About 60% (i.e., 159) galaxies in our sample are fitted well with a single exponential disk model without any conspicuous bulge component. Visual inspection of their morphologies suggests that these LSBs are either smooth disks or irregulars without any brighter central part. The top panel of Figure 3 shows a typical example of these bulgeless LSB

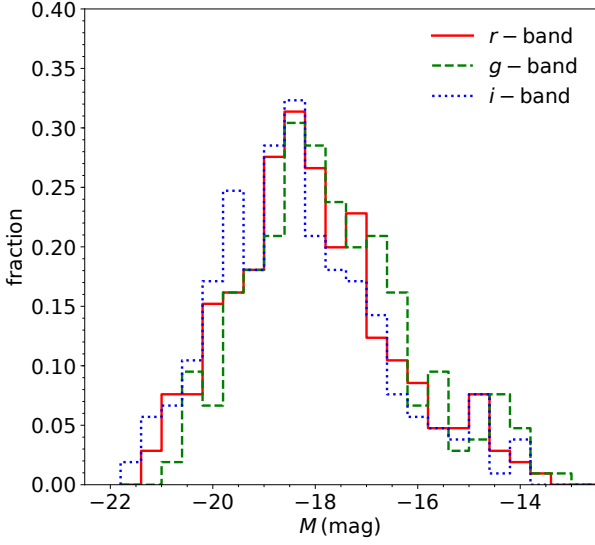


Figure 4. Histogram of the absolute magnitudes of the galaxies in our sample in three bands, namely r , g and i as shown by red (solid), green (dashed) and blue (dotted) lines respectively. The absolute magnitude here corresponds to the combined magnitude of the bulge and disk components of the galaxies.

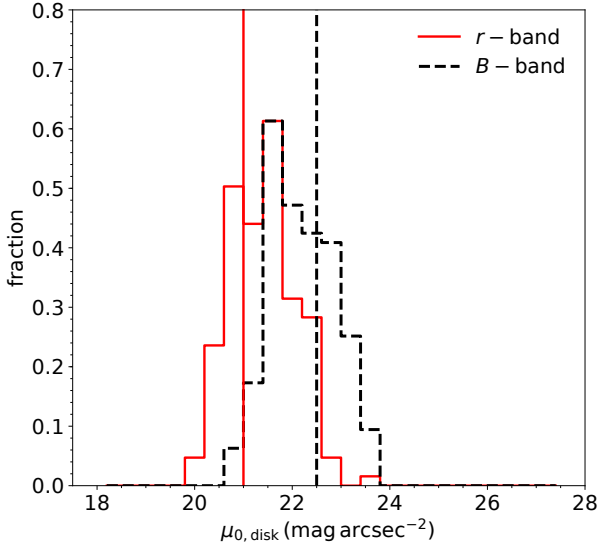


Figure 5. *Bulgeless LSB galaxies*: histogram of the disk central surface brightness (μ_0) of the galaxies in our sample in r and B bands as shown by red (solid) and black (dash-dotted) lines respectively. We have only shown those galaxies where *only disk* component fitting has been done using GALFIT software. The vertical solid (red) and dashed (black) lines correspond to the thresholds of μ_0 being 21 and 22.5 mag arc/sec² in r and B bands, i.e., galaxies lying to the right of these lines in the distribution are LSB galaxies.

galaxies and their 2D decomposition in the r -band. Figure 5 shows their distribution of central surface brightness. The vertical solid (red) and dashed (black) lines correspond to the thresholds of μ_0 being 21 and 22.5 mag arc/sec² in r and B bands respectively. The galaxies lying on the right of these lines are classified as LSBs, and 81% galaxies in

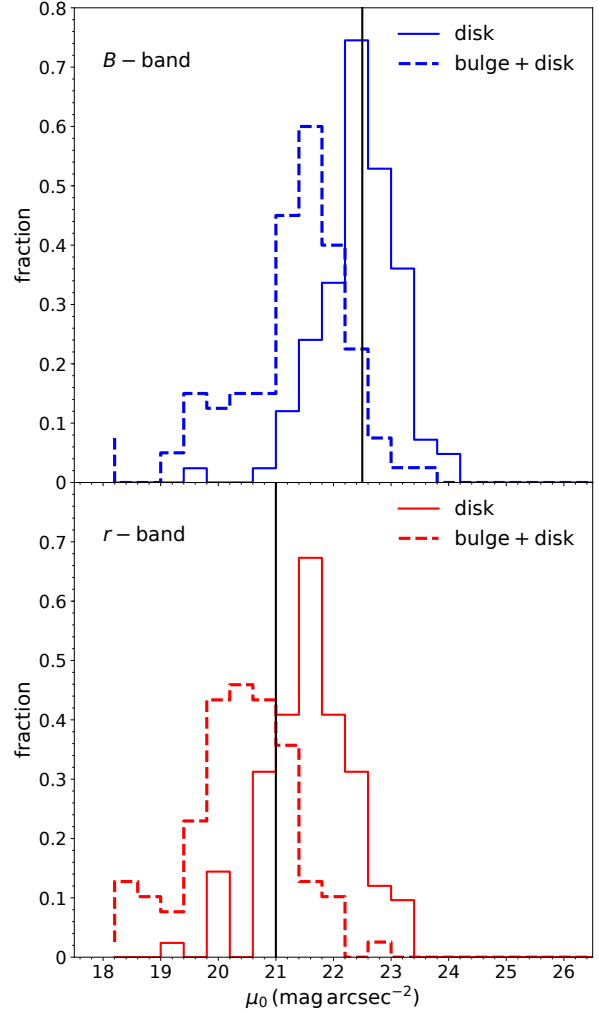


Figure 6. Same as in Figure 5 but for the *LSB galaxies with bulges*. The disk and total (bulge+disk) central surface brightness (μ_0) of the galaxies in our sample in r (lower panel) and B (upper panel) bands are shown as solid and dashed lines.

our sample are LSBs as per r -band criteria. The median of r -band distribution lies at 21.71 mag /arcsec² and that of B -band lies at 22.51 mag /arcsec². The medians of μ_0 distributions for g and i bands lie at 22.11 and 21.56 mag /arcsec² respectively. It is worth mentioning here that the population of bulgeless galaxies in the local universe are not only limited to HSB but also exist in the LSB regime. According to [Kautsch \(2009\)](#), the fraction of bulgeless galaxies in edge-on projection is about 15%. [Fisher & Drory \(2011\)](#) also quotes $\sim 35\%$ of their sample as bulgeless disk galaxies. Finding these large-sized disks with no bulges in the local universe therefore challenges our understanding of galaxy formation in the hierarchical framework ([White & Rees 1978](#)). Since LSBs are generally found in isolated or rather less dense environments, they might have possibly avoided mergers otherwise their disks would have some amount of bulge component and pure exponential profile would be hard to maintain ([Hopkins et al. 2010](#); [Stinson et al. 2013](#); [Naab et al. 2014](#)). Even if an LSB galaxy avoided mergers, internally driven secular evolution (due to non-axisymmetric features in the

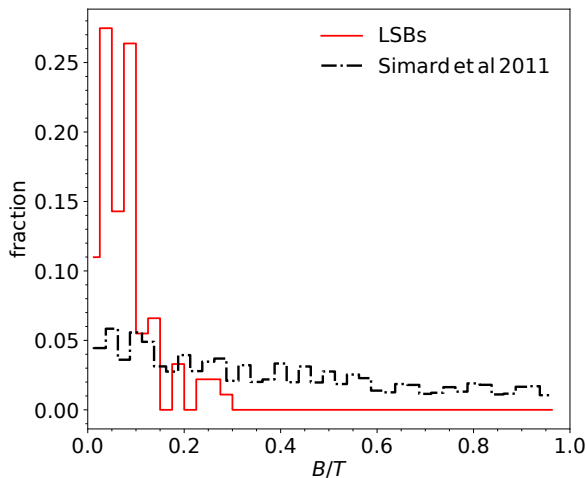


Figure 7. Bulge-to-total (B/T) ratios for our LSB sample and Simard et al 2011 sample. Around 80% of galaxies in our sample have B/T less than 0.1.

early phase of evolution) is inevitable and would produce central concentration or a bulge component (Lynden-Bell & Kalnajs 1972; Kormendy & Kennicutt 2004; Kormendy 2015).

Recently, several cosmological hydrodynamical simulations have succeeded in producing reasonable disk galaxies; but maintaining them as bulgeless over longer period has remained as a harder task, most galaxies end up with $B/T \sim 0.3$, if not more (Governato et al. 2010; Agertz et al. 2011; Guedes et al. 2011; Brook et al. 2012; Marinacci et al. 2014). In a recent study, a similar fraction of bulgeless pure disks is found at $z \sim 1$ (by Sachdeva & Saha 2016) but these were rather massive, bright galaxies. The progenitors of these bulgeless LSBs would be interesting to look for in order to understand their early assembly and evolution since then.

3.2 LSB galaxies with bulges

For the rest of the galaxies ($\sim 40\%$ i.e., 104) in our sample, we were able to model the observed light distribution with two components, namely a bulge and disk (as explained above). In Figure 6, we show the distribution of the central surface brightness derived from the modelling. Due to the presence of the bulge component, the central surface brightness of these galaxies are brighter. If we use the total central surface brightness (as shown by the dashed line in Figure 6), the fraction of qualified LSBs obviously reduces. A comparison of disk μ_0 with the threshold dictates that $\sim 84\%$ galaxies in this sample (where two component fitting has been done) are LSBs. However, this fraction reduces to 61% when the central surface brightness is governed by the full profile of both bulge and disk components.

Figure 7 shows the bulge-to-total ratio (B/T) for our LSB sample galaxies and the all-galaxy population of Simard et al. (2011) in the r -band. About 20% of galaxies in our sample have B/T more than 0.1. Although majority of the

LSBs are with $B/T < 0.1$, it is surprising to see some of these are having significant bulge light.

3.3 Disk scale-length vs central surface brightness

The exponential (disk) scale length (R_s) of a galaxy is a fundamental structural parameter to model its dynamics and to constrain its formation mechanisms. Since LSB galaxies are believed to have different formation mechanisms than HSB galaxies (Bothun et al. 1997), it motivates us to examine the correlation (if any) of the central surface brightness and the disk scale length. Figure 8 shows the $\mu_{0,\text{disk}}-R_s$ relation for all the LSB galaxies in our sample in g , r and i bands. The dashed line in each panel shows the $\mu_{0,\text{disk}}-R_s$ relation for the constant disk luminosity and sets the upper limit in $\mu_{0,\text{disk}}-R_s$ plane as there can not be galaxies with the large scale-lengths and high central surface brightness. The constant disk luminosity lines to constrain the degeneracy of $\mu_{0,\text{disk}}$ and scale-length was first used by Grosbol (1985). Figure 8 shows that there is no apparent correlation between $\mu_{0,\text{disk}}$ and R_s for our sample LSB galaxies and this result is consistent with a number of other studies (Impey et al. 1988; Davies et al. 1988; Irwin et al. 1990; McGaugh & Bothun 1994; Zhong et al. 2008). However, there is a tendency for the galaxies with the largest R_s to be clustered in the low surface density regime and thus with low $\mu_{0,\text{disk}}$. In other words, the fainter LSB galaxies are associated with larger scale lengths. This has also been seen by McGaugh et al. (1995a); de Jong (1996); Fathi (2010). Apparently, most of these galaxies with large scale-lengths are quite isolated. This isolation helps them surviving against tidal interactions and mergers activities. It also seems that these large objects must have proceeded by the gradual accretion without any violent star formation or disruption by neighbouring systems (Bothun et al. 1993; McGaugh & Bothun 1994) so that they could collapse into a single object with low surface density rather than fragmenting into smaller objects.

3.4 Colour-Magnitude Relation

The colour-magnitude relation (CMR) is a powerful tool to understand the underlying stellar population and evolution of galaxies (Holmberg 1958; Roberts & Haynes 1994).

Figure 9 depicts the CMR for our LSB sample (marked as green circle and magenta square symbols) over plotted on the ‘‘all-galaxy’’ sample. The top panel shows the distribution of the r -band absolute magnitudes for our LSB sample (dashed line) and all-galaxy sample (solid line). The right-hand side panel shows the distributions of $g-r$ colour for our LSBs and all-galaxy sample. From this figure, it is clear that our LSB sample peaks at around $g-r \sim 0.4$ which is on the blue side. Indeed, if we use $(g-r)_{\text{cut}} = 0.65 - 0.03(M_r + 20)$ (Blanton et al. 2005) to divide our LSB sample into red and blue populations, the dominant population of our sample galaxies is blue. The existence of these blue LSBs suggests that they are not just the faded remnants of the HSBs. When compared to the SDSS all-galaxy sample, these LSB galaxies occupy the bluer region of the colour-magnitude diagram. It remains to determine what fraction of our sample LSB galaxies is faint. A natural boundary between the bright and faint galaxies is the absolute magnitude (M_*) corresponding

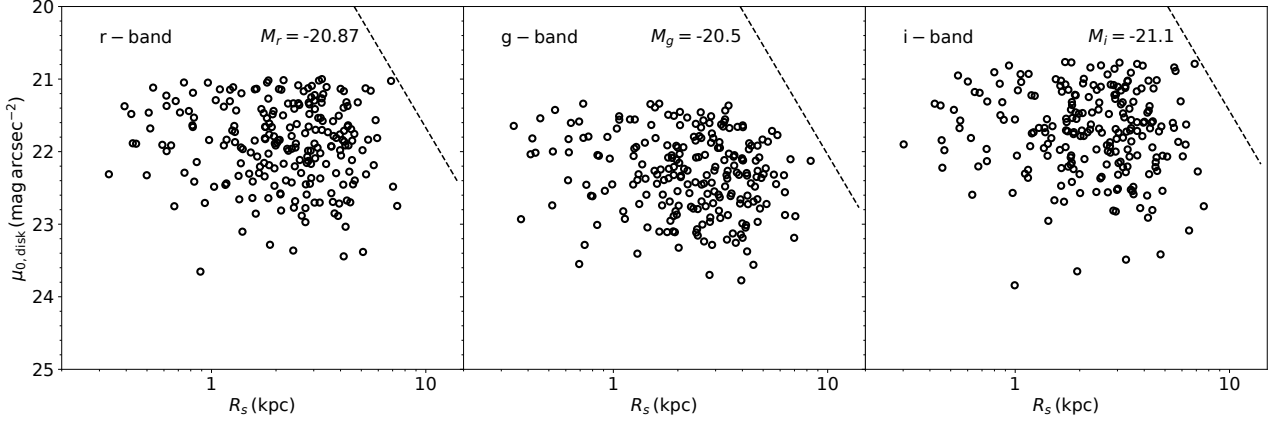


Figure 8. The central surface brightness $\mu_{0,\text{disk}}$ versus scale-length R_s of the LSB galaxies by considering disk *only* components in r -band (left panel), g -band (middle panel) and i -band (right panel). The dashed lines correspond to the exponential disks with constant absolute luminosity of indicated magnitudes in each panel. The equality lines of other magnitudes lie parallel to the dashed line.

to an L_* galaxy, appearing in the Schechter luminosity function (Blanton et al. 2003). We classify a LSB galaxy as faint if its absolute magnitude is larger than $M_* + 2$ (Hollosi & Efstathiou 1988). Based on the SDSS r -band local luminosity function, we have $M_* = -20.66$ (Blanton et al. 2003) or -20.71 according to the GAMA survey (Loveday et al. 2015). According to this criteria, about 71 % of our sample LSB galaxies are on the faint side; some are as faint as $M_r \sim -14$ and can definitely be classified as ultra-faint. Figure 9 shows the location of our barred and unbarred LSBs on the CMR. Most of the barred and unbarred LSBs are blue in our sample and shows no preference for the colour. However, Masters et al. (2011) has found an increase in bar fraction in redder galaxies.

Figure 10 shows the bar fraction of LSB galaxies as a function of r -band absolute magnitude. The barred galaxies are systematically brighter than the unbarred galaxies. This implies that there is higher probability of finding bars in luminous galaxies. There are also 7 red LSBs in our sample and 1 of them has bar in it. In the section below, we will return to the case of barred LSB population.

3.5 Correlation between colour, stellar mass and central surface brightness

In Figure 11, we present the correlation between various structural properties such as central surface brightness, colours and stellar mass of galaxies. Stellar masses are calculated following the Bell et al. (2003) prescription. In that, we compute the r -band mass-to-light ratios $(M/L)_r$ for our sample galaxies using the $g-r$ colour. The left panel shows the $\mu_{0,\text{disk}}$ vs $g-r$ colour of the sample LSB galaxies. As mentioned above, most of our LSB galaxies are blue, but with a wide variation in their central surface brightness. Further, the central surface brightness shows no correlation with the host galaxy stellar mass (see the right panel). The middle panel shows the scatter plot of the stellar mass and the $g-r$ colour for our LSB galaxies. As it seems, there is

a slight tendency that high stellar mass LSB galaxies, on an average, are redder in colour.

From the middle panel of Figure 11, we see a weak trend in the incidence of a bar and $g-r$ colour and the host galaxy stellar mass. Bars seem to be associated with higher stellar mass and $g-r$ colour, although most galaxies in our sample are bluer. Such a trend amongst our LSB galaxies is in compliance with late type spirals (see Barazza et al. 2008; Masters et al. 2011). The faintest barred LSB galaxy in our sample has disk central surface brightness ~ 23.28 mag/arcsec² and its colour is on the bluer side.

Further, we find no correlation on the incidence of a bar with the host galaxy central surface brightness. As bars are known to exist in galaxies with little or no classical bulge (e.g., our MW), the incidence of a bar may not entirely be decided by the pre-existing bulge. But when HSB and LSB galaxies are compared, bars are seen more prominently in HSB galaxies rather than in LSB galaxies (Masters et al. 2011, see). However, in our LSB sample for which the disk central surface brightness varies from 24 - 21 mag/arcsec², we do not find any preference regarding the incidence of a bar.

4 BARRED LSB GALAXIES VS HI GAS MASS

The presence of gas plays a major role in the formation of bars in disk galaxies. Numerical simulations have demonstrated that as the gas fraction increases, the bars get weaker and when the fraction is close to unity or more, simulations end up with almost no bar (Athanasoula et al. 2013). Earlier studies have shown that dissipative effect of gas might even lead to the bar destruction (Bournaud & Combes 2002). Keeping this in mind, we investigate the incidence of bars in LSB galaxies in the presence of cold neutral hydrogen gas measured by the Green Bank Telescope (Schneider et al. 1992). Only 85 galaxies in our LSB sample have reliable HI observations and these are shown in Figure 12. It is clear that there is a strong correlation between the stellar mass and HI

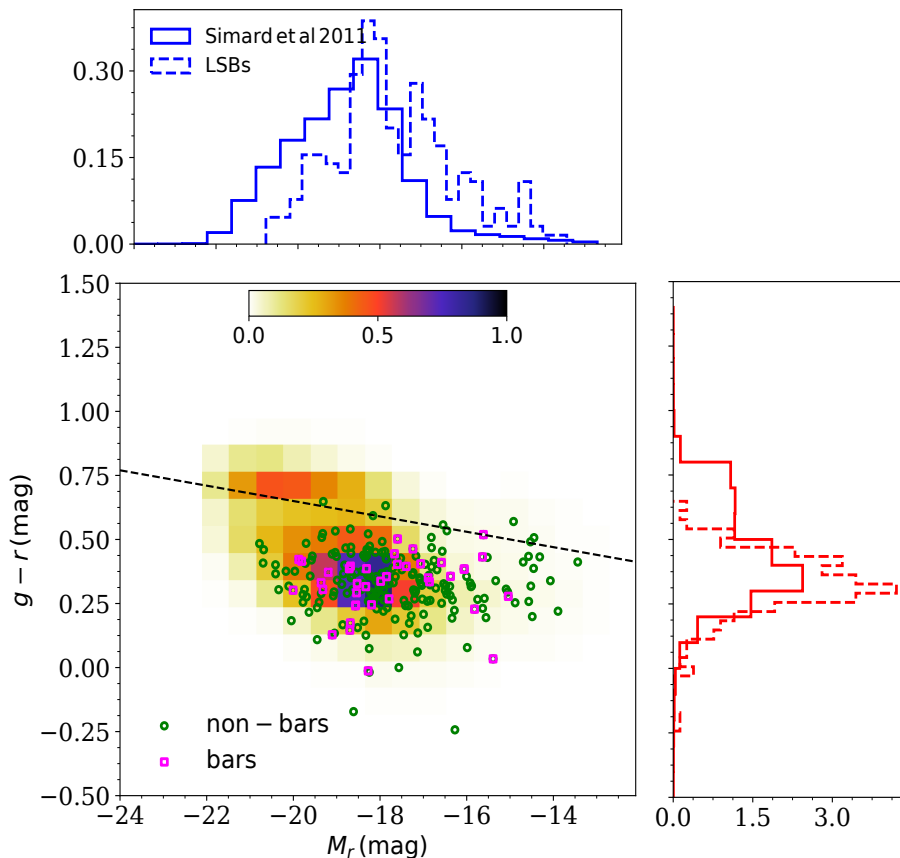


Figure 9. The colour-magnitude diagram (CMD) of the LSB galaxies. This uses $g-r$ colours and the r -band absolute magnitudes of our LSB sample galaxies and all galaxy (Simard et al 2011) sample. In the middle panel, we show bars in our sample as magenta squares and all other galaxies as green circles. The density contours represent the all galaxy (Simard et al 2011) sample. This is over-plotted in order to compare our galaxies with the all galaxy sample. The black dashed line divides the sample into red and blue based on colour-cut. The top panel shows the distributions of r -band absolute magnitudes of our LSB sample galaxies (dashed line) and all-galaxy sample galaxies (solid line) whereas the right-hand side panel shows the distributions of $g-r$ colours where lines denote the same samples as that of top panel.

gas mass for our LSB galaxies. Most of these LSB galaxies are very gas-rich, with gas fraction $f_{gas} = M_{HI}/M_* > 1$ (Figure 13). Of the 85 LSBs, there are 4 red LSBs and the rest are blue. *We see bars both in red and blue LSB galaxies. Irrespective of their colours, the incidence of a bar is associated with high gas fraction in our sample.* Not only that, we have about 37 blue LSBs hosting bars - this implies that about 15% of the blue LSB galaxies in our sample host bars - this number is in sync with other recent studies (Masters et al. 2012; Cervantes Sodi & Sánchez García 2017) based on large volume limited sample drawn from SDSS DR7. These studies and a number of others have shown that this fraction is lower than that in gas-poor spirals (Eskridge et al. 2000; Barazza et al. 2008; Masters et al. 2011). However, according to a recent study (Erwin 2018), bars are common in both gas-rich blue galaxies as well as in gas-poor red spirals. It remains to be understood what makes bar formation possible in such gas-rich (with $f_{gas} \gtrsim 1$) blue LSB galaxies.

5 DISCUSSION AND CONCLUSIONS

We have studied a sample of 263 LSB galaxies observed by Green Bank Telescope (Schneider et al. 1992) which are in overlap with the SDSS footprint. We have performed two-component bulge-disk decomposition of 263 galaxies in the SDSS g , r and i bands and investigated their structural properties in detail. We have found that 60% LSBs in our specific sample are bulgeless while 40% are with bulges. Some of the LSBs are associated with significant bulge component with $B/T > 0.1$. Since LSBs are known to be dwelling in less dense environment (Rosenbaum & Bomans 2004), mergers and interactions are unlikely to have led the bulge formation. We also have 15% barred galaxies in our sample. Our findings of bulges and bars suggest a considerable on-going evolution in the local LSB galaxies and the bars might as well be playing a role in the bulge growth (Laurikainen et al. 2007; Gadotti 2011; Cheung et al. 2013). The interesting fact about our sample is that they are not the class of giant LSB galaxies, in fact, most of our LSBs are faint, blue and gas-rich and roughly half of them are hosting bars and bulges.

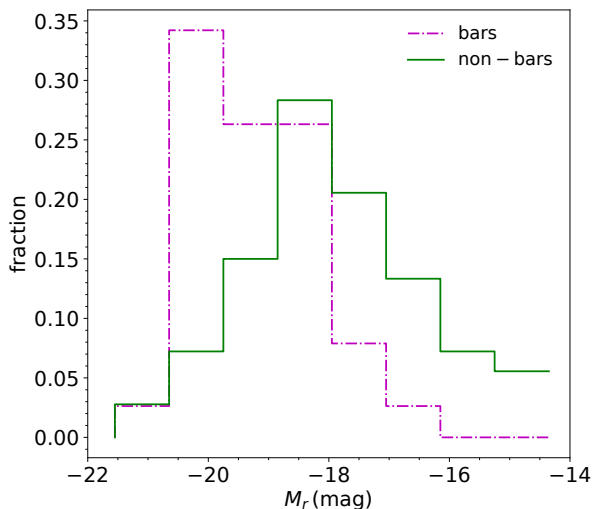


Figure 10. This figure shows the histogram of absolute r -band magnitude of barred and unbarred galaxies. The barred galaxies are systematically brighter than the unbarred galaxies.

Since LSB galaxies are dark matter dominated, disks are known to be stable against bar formation (Ostriker & Peebles 1973; Efstathiou et al. 1982; Christodoulou et al. 1995; Cervantes Sodi et al. 2015; Algorry et al. 2017), as shown in numerical simulations of stellar disks with dark matter dominance at all radii (Saha 2014). Question arises how these faint blue LSBs are making bars and bulges. One possibility is that LSB disks are embedded in dark matter halos that are spinning (Jimenez et al. 1998; Vitvitska et al. 2002; Kim & Lee 2013) which might be promoting bar formation provided spin parameter is not too high (Saha & Naab 2013; Cervantes-Sodi et al. 2013; Long et al. 2014; Collier et al. 2017). Whether these bars lead to the formation of bulges or other processes such as minor mergers being involved, needs further and detailed investigation.

Major conclusions from our work on this *specific* sample are:

- We classify a galaxy as LSB if its r -band disk central surface brightness is fainter than $21 \text{ mag arcsec}^{-2}$. According to the threshold criterion, $\sim 84\%$ galaxies in our sample are LSB. This fraction reduces further to 61% when the central surface brightness of the full galaxy light distribution is used.

- The median scale-length of LSB sample galaxies is 2.4 kpc which is comparable to the full galaxy population (average $\sim 3.79 \text{ kpc}$) as shown by Fathi et al. (2010). We have found no correlation between the scale length and disk central surface brightness.

- There seems to be a weak correlation between the colour and stellar mass of these LSB galaxies.

- Dominant fraction of galaxies in our sample is faint, with absolute magnitude as faint as -14 . This sample of faint LSBs is rich in morphology.

- Most of our LSB galaxies are blue as per $g-r$ colour criteria. However, there are also 7 red LSBs in our sample.

- Based on the bulge-disk decomposition, we have found that 40% of our sample LSBs are with bulges and of these, there are $\sim 20\%$ with $B/T > 0.1$.

- We have found that $\sim 15\%$ LSBs in our sample are barred. Bars are seen in both red and blue LSBs in our sample. The incidence of a bar has no correlation on the host galaxy central surface brightness. Most of these barred LSBs are highly gas-rich and blue.

ACKNOWLEDGMENTS

We thank the anonymous referee for a careful reading and insightful comments on the manuscript. The research of IP is supported by the INSPIRE Faculty grant (DST/INSPIRE/04/2016/000404) awarded by the Department of Science and Technology, Government of India.

SDSS is managed by the Astrophysical Research Consortium for the Participating Institutions of the SDSS Collaboration including the Brazilian Participation Group, the Carnegie Institution for Science, Carnegie Mellon University, the Chilean Participation Group, the French Participation Group, Harvard-Smithsonian Center for Astrophysics, Instituto de Astrofísica de Canarias, The Johns Hopkins University, Kavli Institute for the Physics and Mathematics of the Universe (IPMU) / University of Tokyo, Lawrence Berkeley National Laboratory, Leibniz Institut für Astrophysik Potsdam (AIP), Max-Planck-Institut für Astronomie (MPIA Heidelberg), Max-Planck-Institut für Astrophysik (MPA Garching), Max-Planck-Institut für Extraterrestrische Physik (MPE), National Astronomical Observatories of China, New Mexico State University, New York University, University of Notre Dame, Observatório Nacional / MCTI, The Ohio State University, Pennsylvania State University, Shanghai Astronomical Observatory, United Kingdom Participation Group, Universidad Nacional Autónoma de México, University of Arizona, University of Colorado Boulder, University of Oxford, University of Portsmouth, University of Utah, University of Virginia, University of Washington, University of Wisconsin, Vanderbilt University, and Yale University.

We have also used PyRAF for our study, a product of the Space Telescope Science Institute, which is operated by AURA for NASA.

REFERENCES

- Adami C., et al., 2006, *A&A*, **459**, 679
 Agertz O., Teyssier R., Moore B., 2011, *MNRAS*, **410**, 1391
 Algorry D. G., et al., 2017, *MNRAS*, **469**, 1054
 Athanassoula E., Machado R. E. G., Rodionov S. A., 2013, *MNRAS*, **429**, 1949
 Barazza F. D., Jogee S., Marinova I., 2008, *ApJ*, **675**, 1194
 Barth A. J., 2007, *AJ*, **133**, 1085
 Beijersbergen M., de Blok W. J. G., van der Hulst J. M., 1999, *A&A*, **351**, 903
 Bell E. F., McIntosh D. H., Katz N., Weinberg M. D., 2003, *ApJS*, **149**, 289
 Blanton M. R., et al., 2003, *ApJ*, **592**, 819
 Blanton M. R., Lupton R. H., Schlegel D. J., Strauss M. A., Brinkmann J., Fukugita M., Loveday J., 2005, *ApJ*, **631**, 208
 Blanton M. R., Kazin E., Muna D., Weaver B. A., Price-Whelan A., 2011, *AJ*, **142**, 31
 Bothun G. D., Beers T. C., Mould J. R., Huchra J. P., 1985, *AJ*, **90**, 2487

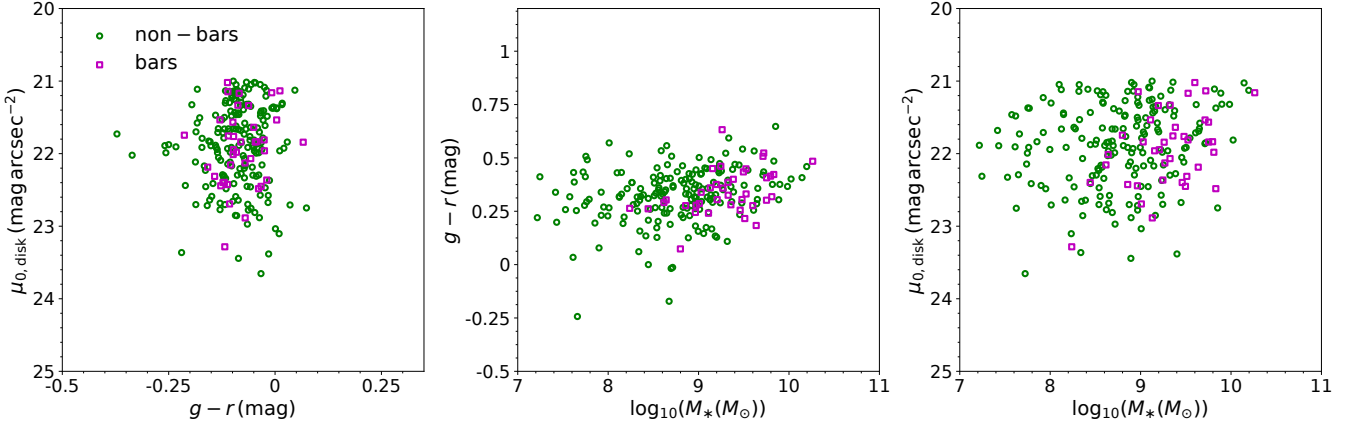


Figure 11. This figure shows the relation between different structural properties of LSB galaxies. The left and middle panel show the scatter plot between the r -band μ_0 and the stellar masses of the galaxies with the $g-r$ colours whereas the right panel shows the correlation between r -band disk μ_0 and stellar masses of galaxies.

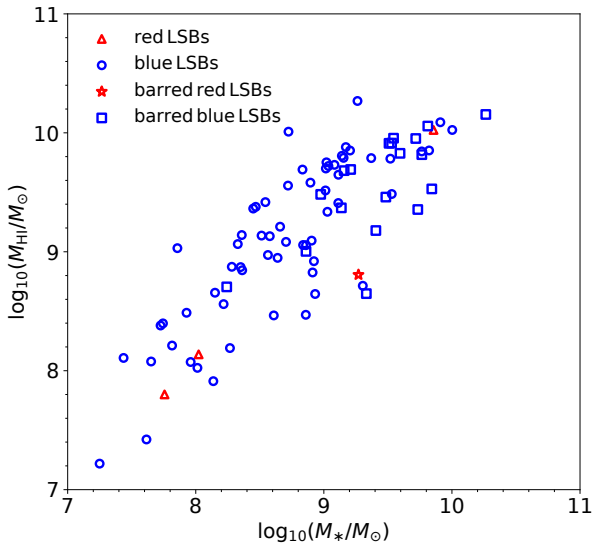


Figure 12. Stellar mass versus HI mass of the LSB galaxies in our sample. The blue and red LSB galaxies are shown as blue circles and red triangles whereas the barred red and blue galaxies are marked by red stars and blue squares.

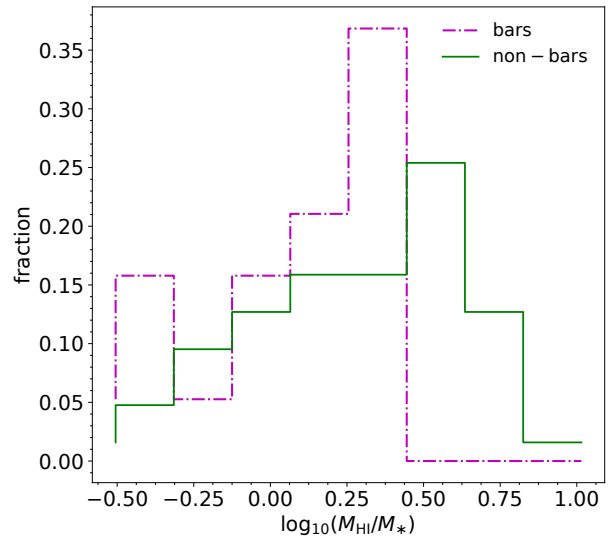


Figure 13. Histogram of HI mass to stellar mass of the LSB galaxies in our sample. Most of the galaxies in our sample are gas-rich.

Bothun G. D., Schombert J. M., Impy C. D., Sprayberry D., McGaugh S. S., 1993, *AJ*, **106**, 530
 Bothun G., Impy C., McGaugh S., 1997, *PASP*, **109**, 745
 Bournaud F., Combes F., 2002, *A&A*, **392**, 83
 Boyle B. J., Shanks T., Peterson B. A., 1988, *MNRAS*, **235**, 935
 Brook C. B., Stinson G., Gibson B. K., Roškar R., Wadsley J., Quinn T., 2012, *MNRAS*, **419**, 771
 Brown W. R., Geller M. J., Fabricant D. G., Kurtz M. J., 2001, *AJ*, **122**, 714
 Cervantes Sodi B., Sánchez García O., 2017, *ApJ*, **847**, 37
 Cervantes-Sodi B., Li C., Park C., Wang L., 2013, *ApJ*, **775**, 19
 Cervantes Sodi B., Li C., Park C., 2015, *ApJ*, **807**, 111
 Cheung E., et al., 2013, *ApJ*, **779**, 162
 Christodoulou D. M., Shlosman I., Tohline J. E., 1995, *ApJ*, **443**, 551

Collier A., Shlosman I., Heller C., 2017, preprint, ([arXiv:1712.02802](https://arxiv.org/abs/1712.02802))
 Courteau S., 1996, *ApJS*, **103**, 363
 Davies J. I., Phillipps S., Cawson M. G. M., Disney M. J., Kibblewhite E. J., 1988, *MNRAS*, **232**, 239
 Dominguez-Tenreiro R., Alimi J.-M., Serna A., Thuan T. X., 1996, *ApJ*, **469**, 53
 Duc P.-A., et al., 2015, *MNRAS*, **446**, 120
 Efstathiou G., Lake G., Negroponete J., 1982, *MNRAS*, **199**, 1069
 Erwin P., 2018, *MNRAS*, **474**, 5372
 Eskridge P. B., et al., 2000, *AJ*, **119**, 536
 Fathi K., 2010, *ApJ*, **722**, L120
 Fathi K., Allen M., Boch T., Hatziminaoglou E., Peletier R. F., 2010, *MNRAS*, **406**, 1595
 Fisher D. B., Drory N., 2011, *ApJ*, **733**, L47
 Freeman K. C., 1970, *ApJ*, **160**, 811

- Gadotti D. A., 2011, *MNRAS*, **415**, 3308
- Galaz G., Villalobos A., Infante L., Donzelli C., 2006, *AJ*, **131**, 2035
- Galaz G., Herrera-Camus R., Garcia-Lambas D., Padilla N., 2011, *ApJ*, **728**, 74
- Ghosh S., Jog C. J., 2014, *MNRAS*, **439**, 929
- Governato F., et al., 2010, *Nature*, **463**, 203
- Graham A. W., Driver S. P., 2005, *PASA*, **22**, 118
- Greco J. P., et al., 2017, preprint, ([arXiv:1709.04474](https://arxiv.org/abs/1709.04474))
- Grosbol P. J., 1985, *A&AS*, **60**, 261
- Guedes J., Callegari S., Madau P., Mayer L., 2011, *ApJ*, **742**, 76
- Hogg D. W., Baldry I. K., Blanton M. R., Eisenstein D. J., 2002, *ArXiv Astrophysics e-prints*,
- Hollosi J., Efstathiou G., 1988, in Seitter W. C., Duerbeck H. W., Tacke M., eds, *Lecture Notes in Physics*, Berlin Springer Verlag Vol. 310, Large-scale structures in the universe. pp 106–110, [doi:10.1007/3-540-50135-5_62](https://doi.org/10.1007/3-540-50135-5_62)
- Holmberg E., 1958, *Meddelanden fran Lunds Astronomiska Observatorium Serie II*, **136**, 1
- Honey M., Das M., Ninan J. P., Manoj P., 2016, *MNRAS*, **462**, 2099
- Honey M., van Driel W., Das M., Martin J.-M., 2018, *MNRAS*, **471**, 1131
- Hopkins P. F., Kereš D., Ma C.-P., Quataert E., 2010, *MNRAS*, **401**, 1131
- Huang S., et al., 2014, *ApJ*, **793**, 40
- Impey C., Bothun G., 1997, *ARA&A*, **35**, 267
- Impey C., Bothun G., Malin D., 1988, *ApJ*, **330**, 634
- Impey C. D., Sprayberry D., Irwin M. J., Bothun G. D., 1996, *ApJS*, **105**, 209
- Irwin M. J., Davies J. I., Disney M. J., Phillipps S., 1990, *MNRAS*, **245**, 289
- Jimenez R., Padoan P., Matteucci F., Heavens A. F., 1998, *MNRAS*, **299**, 123
- Kautsch S. J., 2009, *Astronomische Nachrichten*, **330**, 100
- Kim J.-h., Lee J., 2013, *MNRAS*, **432**, 1701
- Kim K., Oh S., Jeong H., Aragón-Salamanca A., Smith R., Yi S. K., 2016, *ApJS*, **225**, 6
- Kniazev A. Y., Grebel E. K., Pustilnik S. A., Pramskij A. G., Kniazeva T. F., Prada F., Harbeck D., 2004, *AJ*, **127**, 704
- Kormendy J., 2015, *Highlights of Astronomy*, **16**, 316
- Kormendy J., Kennicutt Jr. R. C., 2004, *ARA&A*, **42**, 603
- Kuzio de Naray R., McGaugh S. S., de Blok W. J. G., 2004, *MNRAS*, **355**, 887
- Lackner C. N., Gunn J. E., 2012, *MNRAS*, **421**, 2277
- Laurikainen E., Salo H., Buta R., Knapen J. H., 2007, *MNRAS*, **381**, 401
- Lelli F., Fraternali F., Sancisi R., 2010, *A&A*, **516**, A11
- Long S., Shlosman I., Heller C., 2014, *ApJ*, **783**, L18
- Loveday J., et al., 2015, *MNRAS*, **451**, 1540
- Lynden-Bell D., Kalnajis A. J., 1972, *MNRAS*, **157**, 1
- Marinacci F., Pakmor R., Springel V., 2014, *MNRAS*, **437**, 1750
- Masters K. L., et al., 2011, *MNRAS*, **411**, 2026
- Masters K. L., et al., 2012, *MNRAS*, **424**, 2180
- Mayer L., Wadsley J., 2004, *MNRAS*, **347**, 277
- McGaugh S., 1996, in Bender R., Davies R. L., eds, *IAU Symposium Vol. 171, New Light on Galaxy Evolution*. p. 97 ([arXiv:astro-ph/9507058](https://arxiv.org/abs/astro-ph/9507058))
- McGaugh S. S., Bothun G. D., 1994, *AJ*, **107**, 530
- McGaugh S. S., Schombert J. M., Bothun G. D., 1995a, *AJ*, **109**, 2019
- McGaugh S. S., Bothun G. D., Schombert J. M., 1995b, *AJ*, **110**, 573
- Meert A., Vikram V., Bernardi M., 2015, *MNRAS*, **446**, 3943
- Mihos J. C., McGaugh S. S., de Blok W. J. G., 1997, *ApJ*, **477**, L79
- Morelli L., Corsini E. M., Pizzella A., Dalla Bontà E., Coccato L., Méndez-Abreu J., Cesetti M., 2012, *MNRAS*, **423**, 962
- Naab T., et al., 2014, *MNRAS*, **444**, 3357
- Nilson P., 1973, *Uppsala general catalogue of galaxies*
- O’Neil K., Bothun G., 2000, *ApJ*, **529**, 811
- O’Neil K., Andreon S., Cuillandre J.-C., 2003a, *A&A*, **399**, L35
- O’Neil K., Schinnerer E., Hofner P., 2003b, *ApJ*, **588**, 230
- Oke J. B., 1974, *ApJS*, **27**, 21
- Ostriker J. P., Peebles P. J. E., 1973, *ApJ*, **186**, 467
- Peng C. Y., Ho L. C., Impey C. D., Rix H.-W., 2002, *AJ*, **124**, 266
- Peng C. Y., Ho L. C., Impey C. D., Rix H.-W., 2010, *AJ*, **139**, 2097
- Pickering T. E., Impey C. D., van Gorkom J. H., Bothun G. D., 1997, *AJ*, **114**, 1858
- Pizzella A., Corsini E. M., Sarzi M., Magorrian J., Méndez-Abreu J., Coccato L., Morelli L., Bertola F., 2008, *MNRAS*, **387**, 1099
- Roberts M. S., Haynes M. P., 1994, *ARA&A*, **32**, 115
- Rosenbaum S. D., Bomans D. J., 2004, *A&A*, **422**, L5
- Rosenbaum S. D., Krusch E., Bomans D. J., Dettmar R.-J., 2009, *A&A*, **504**, 807
- SDSS Collaboration et al., 2016, preprint, ([arXiv:1608.02013](https://arxiv.org/abs/1608.02013))
- Sachdeva S., Saha K., 2016, *ApJ*, **820**, L4
- Saha K., 2014, preprint, ([arXiv:1403.1711](https://arxiv.org/abs/1403.1711))
- Saha K., Naab T., 2013, *MNRAS*, **434**, 1287
- Schmidt M., Green R. F., 1983, *ApJ*, **269**, 352
- Schneider S. E., Thuan T. X., Magri C., Wadiak J. E., 1990, *ApJS*, **72**, 245
- Schneider S. E., Thuan T. X., Mangum J. G., Miller J., 1992, *ApJS*, **81**, 5
- Schombert J., Maciel T., McGaugh S., 2011, *Advances in Astronomy*, **2011**, 143698
- Sersic J. L., 1968, *Atlas de Galaxias Australes*
- Simard L., Mendel J. T., Patton D. R., Ellison S. L., McConnachie A. W., 2011, *ApJS*, **196**, 11
- Smith J. A., et al., 2002, *AJ*, **123**, 2121
- Sprayberry D., Impey C. D., Bothun G. D., Irwin M. J., 1995, *AJ*, **109**, 558
- Stinson G. S., Brook C., Macciò A. V., Wadsley J., Quinn T. R., Couchman H. M. P., 2013, *MNRAS*, **428**, 129
- Thuan T. X., Alimi J.-M., Gott III J. R., Schneider S. E., 1991, *ApJ*, **370**, 25
- Trujillo I., Fliri J., 2016, *ApJ*, **823**, 123
- Vitvitska M., Klypin A. A., Kravtsov A. V., Wechsler R. H., Primack J. R., Bullock J. S., 2002, *ApJ*, **581**, 799
- White S. D. M., Rees M. J., 1978, *MNRAS*, **183**, 341
- York D. G., et al., 2000, *AJ*, **120**, 1579
- Zhong G. H., Liang Y. C., Liu F. S., Hammer F., Hu J. Y., Chen X. Y., Deng L. C., Zhang B., 2008, *MNRAS*, **391**, 986
- de Blok W. J. G., McGaugh S. S., 1996, *ApJ*, **469**, L89
- de Blok W. J. G., van der Hulst J. M., 1998, *A&A*, **335**, 421
- de Blok W. J. G., van der Hulst J. M., Bothun G. D., 1995, *MNRAS*, **274**, 235
- de Blok E., McGaugh S., Rubin V., 2001, *ArXiv Astrophysics e-prints*,
- de Jong R. S., 1996, *A&A*, **313**, 45
- van der Hulst J. M., Skillman E. D., Smith T. R., Bothun G. D., McGaugh S. S., de Blok W. J. G., 1993, *AJ*, **106**, 548

APPENDIX A: COMPARISON OF MODEL MAGNITUDES WITH THE SDSS PETROSIAN MAGNITUDES

In this appendix, we give the comparison of magnitudes of the LSB sample galaxies as given by the SDSS with that of what we get from GALFIT decomposition. We convert the r -band GALFIT model magnitudes of LSB galaxies to the AB magnitudes using standard relation (Oke 1974). In

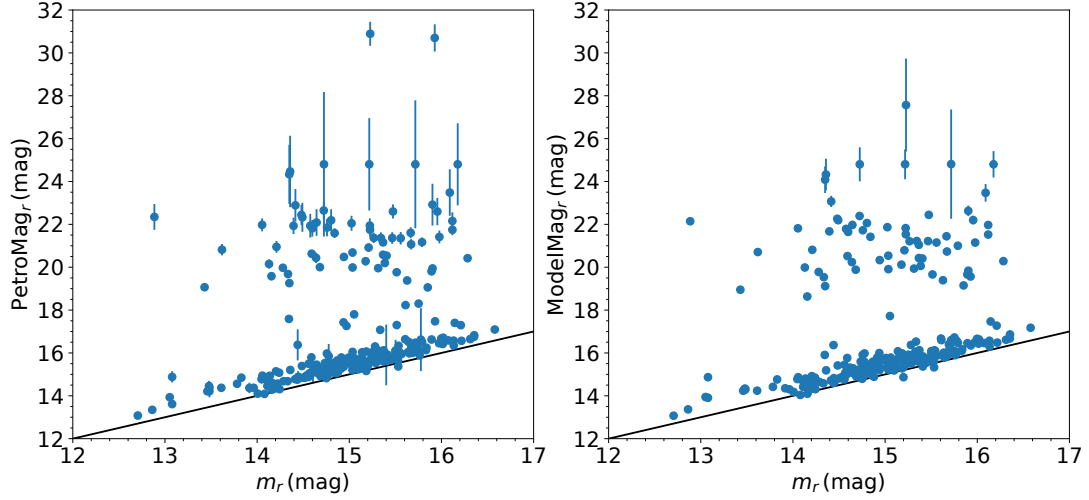


Figure A1. Comparison of SDSS Petrosian (left panel) and model (right panel) magnitudes with the AB magnitudes of LSB sample galaxies in r -band. The AB magnitudes of the sample galaxies are calculated from the flux estimated by the model magnitudes given by GALFIT. The black colour solid line in both panels is 45° line for a better visual comparison.

the left hand panel of Figure A1, we show the comparison of SDSS Petrosian magnitudes and the AB magnitudes of LSB galaxies in r -band whereas the right hand panel depicts the comparison of SDSS model magnitudes with that of AB magnitudes. Galaxies which have r -band Petrosian magnitudes less than 17, are pretty much in agreement with our AB magnitudes of galaxies. However, almost all the galaxies have bit brighter AB magnitudes as compared to their SDSS Petrosian or model magnitudes. There are around $\sim 28\%$ galaxies where the difference between SDSS Petrosian or model magnitudes and AB magnitudes is more than 1 mag. If we consider Petrosian or model magnitudes from SDSS for our analysis, more galaxies would be termed as LSB.